nature physics

ARTICLES

PUBLISHED ONLINE: 13 APRIL 2014 | DOI: 10.1038/NPHYS2933

Hidden spin polarization in inversion-symmetric bulk crystals

Xiuwen Zhang[1,2,3†], Qihang Liu[1,4†], Jun-Wei Luo[3*], Arthur J. Freeman[4] and Alex Zunger[1*]

Spin–orbit coupling can induce spin polarization in nonmagnetic 3D crystals when the inversion symmetry is broken, as manifested by the bulk Rashba and Dresselhaus effects. We establish that these spin-polarization effects originate fundamentally from specific atomic site asymmetries, rather than, as generally accepted, from the asymmetry of the crystal space group. This understanding leads to the recognition that a previously overlooked hidden form of spin polarization should exist in centrosymmetric crystals. Although all energy bands must be doubly degenerate in centrosymmetric materials, we find that the two components of such doubly degenerate bands could have opposite polarizations, each spatially localized on one of the two separate sectors forming the inversion partners. We demonstrate such hidden spin polarizations in particular centrosymmetric crystals by first-principles calculations. This new understanding could considerably broaden the range of currently useful spintronic materials and enable the control of spin polarization by means of operations on the atomic scale.

Much of the recent interest in spintronics[1,2] has been prompted by the fact that when spin–orbit coupling (SOC) occurs in systems with sufficiently low crystalline symmetry, an effective magnetic field $\mathbf{B}_{\text{eff}} \propto [\nabla V(\mathbf{r}) \times \mathbf{p}]$ emerges[3], where $V(\mathbf{r})$ denotes the crystal potential and $\mathbf{p}$ the momentum, that leads to spin splitting and spin polarization even in nonmagnetic materials. This is known in three-dimensional (3D) bulk-periodic solids as the Dresselhaus effect (denoted here as D-1; ref. 4), arising from bulk inversion asymmetry (BIA), and in 2D quantum wells and heterostructures as the Rashba effect[5], arising from 2D structural inversion asymmetry (SIA). However, recent theoretical[6,7] and experimental studies[6] revealed a Rashba-like spin-texture in some 3D bulk crystals (denoted here as R-1), where SIA plays no role, a surprising finding that highlights the incompleteness of our current understanding of the origins of the bulk SOC effects. Indeed, the current view that R-1 and D-1 require the absence of crystal bulk inversion symmetry has also established the generally accepted expectation that it would be unwise to look for spin splitting in a 3D material that has bulk inversion symmetry, a paradigm that has greatly narrowed the playing field of spintronic materials to non-centrosymmetric materials with significant SOC (large atomic numbers).

The central insight here is that because the SOC is a relativistic effect, anchored on particular nuclear sites in the solid[8], it is the symmetry of such individual atomic sites in the solid that forms a good starting point to describe the SOC-induced spin polarization effect, rather than the global symmetry of the unit cell (as in SIA or BIA). The total spin polarization of a crystal is then the (vector) sum over all sites of the local site (Rashba or Dresselhaus) spin polarizations. This simple view not only explains the origin of R-1 and D-1 effects in an unified fashion, but leads immediately to the discovery of two hitherto missing forms of spin polarization in nonmagnetic materials (called here R-2 and D-2), as explained schematically in Fig. 1.

When the site point group of an atom within a 3D crystal lacks inversion symmetry, the atomic site can be either nonpolar or polar—that is, have either an inversion-asymmetric (IA) local environment, or a local environment creating a site dipole-field (DF; ref. 9), respectively. The atomic SOC of that site will then lead in the former case to a local Dresselhaus spin polarization, whereas in the latter case it will lead to a local Rashba spin polarization. When, in addition to these site symmetries, the global bulk space group lacks inversion symmetry (that is, being non-centrosymmetric), the inversion-asymmetric local motifs combine to produce the well-known bulk Dresselhaus (D-1) effect[4], whereas the site dipole-field local motifs combine to produce the bulk Rashba (R-1) effect[5] (Fig. 1b). The R-1 and D-1 effects are characterized by net spin polarizations with their own characteristic spin textures[6,10,11]: generally in R-1 we have a helical texture[10,11], where the spin orients perpendicular to the dipole field axis[6], and in D-1 we have a nonhelical texture.

This insight into how the bulk R-1 and D-1 effects emerge from a superposition of the respective site properties suggests that even when the bulk space group of a solid has inversion symmetry (being centrosymmetric) — a case that would be dismissed as being totally uninteresting from the point of view of spin polarization physics—there can be a hidden spin polarization(Fig. 1c). Imagine, for example, a layered crystal with each of its individual layers ('sectors') having a local symmetry producing a dipole field (thus, a local Rashba spin polarization), but where the crystal as a whole has a space group with inversion symmetry. In this case, the Rashba spin polarization from each local sector (α) is compensated by the other sector—its inversion partner (β). Rather than being intrinsically absent, as normally expected under the current paradigm, this R-2 spin polarization would instead be concealed by compensation. We illustrate such spin polarization with Dresselhaus or Rashba spin textures in centrosymmetric crystals by density functional theory (DFT) calculations: the D-2 effect in NaCaBi, and even in bulk Si (diamond-like structure), and the R-2 effect in $LaOBiS_2$. The relevant energy bands are doubly degenerate because of a combination of bulk inversion symmetry and time reversal symmetry.

[1]University of Colorado, Boulder, Colorado 80309, USA, [2]Colorado School of Mines, Golden, Colorado 80401, USA, [3]National Renewable Energy Laboratory, Golden, Colorado 80401, USA, [4]Department of Physics and Astronomy, Northwestern University, Evanston, Illinois 60208, USA. †These authors contributed equally to this work. *e-mail: jwluo@semi.ac.cn; alex.zunger@colorado.edu

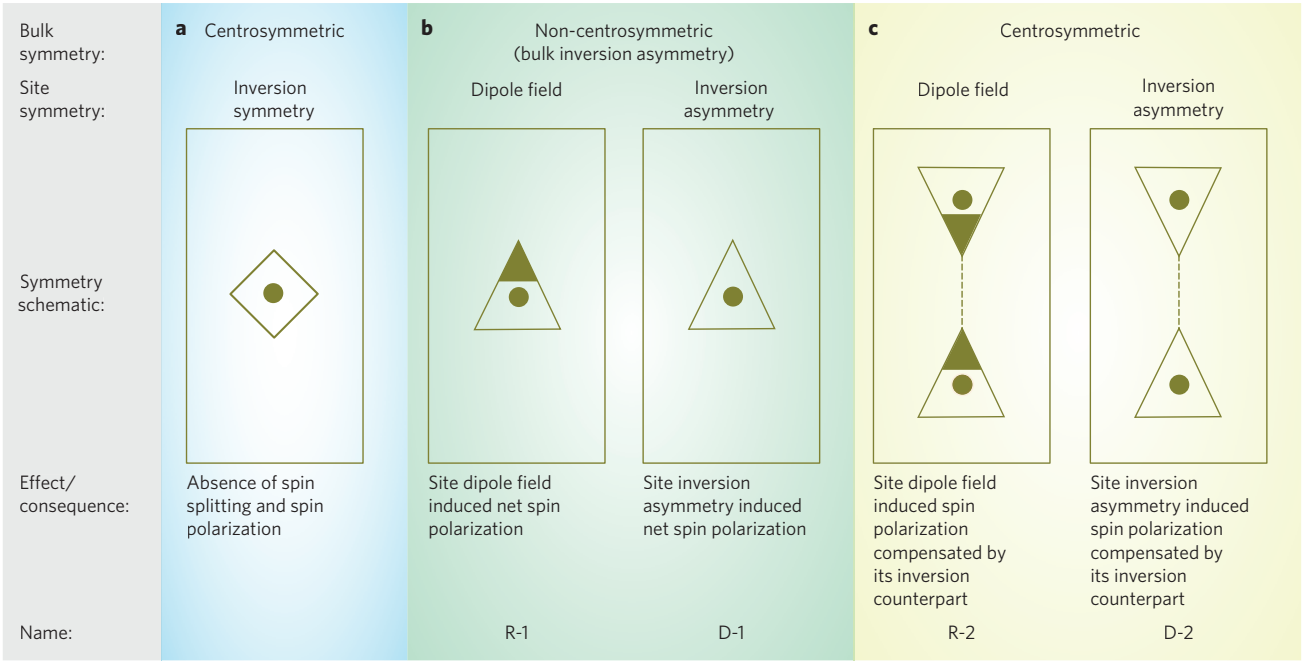

Figure 1 | The three classes of spin polarization in nonmagnetic bulk crystals. a, Absence of spin polarization in centrosymmetric crystals if all atomic sites are inversion symmetric. As the local environment (crystal field) of centrosymmetric atomic sites does not produce spin-orbit coupling induced spin polarization, the total (bulk) spin polarization is absent as well. **b**, Net bulk spin polarizations (R-1 and D-1 effects): a local site dipole field or the site inversion asymmetry leads to local Rashba or local Dresselhaus effects, respectively. In combination with a non-centrosymmetric space group, these local effects produce bulk R-1 (Rashba) and D-1 (Dresselhaus) effects, respectively. **c**, Compensated (hidden) bulk spin polarization (R-2 and D-2 effects): a local site dipole field or the site inversion asymmetry leads to local Rashba or local Dresselhaus effects, respectively, as in **b**. In combination with a centrosymmetric space group, these local effects produce bulk R-2 (Rashba) and D-2 (Dresselhaus) effects, respectively. Here the spin polarization from each sector is concealed by compensation from their inversion partners, but is readily visible when the results from individual sectors are observed.

If two quantum mechanical wavefunctions are degenerate, one can choose their linear combination such that the spin polarization of each state is not unique and only the sum of the spin polarization of the two states is meaningful. A key observation here is that in the R-2 and D-2 effects, the spin polarization of the energetically degenerate bands is spatially segregated into a dominant spin texture for one real-space sector, whereas the opposite spin texture is associated with its inversion partner. This type of R-2 and D-2 doubly degenerate bands is different from the common notion of spin-degenerate bands where both spin-up and spin-down wavefunctions occur in the same real-space sector—that is, there is no spatial separation between two spin-subbands. Such local SOC-induced spin polarization, segregated into different real space domains, is clearly apparent from DFT calculations reported here, because in such calculations the spin degrees of freedom of each bulk state can be projected onto individual real-space sectors.

Bulk symmetry, site symmetry and spin polarization

The basic concepts of symmetry used in this paper are illustrated in Fig. 1. One can distinguish the presence or absence of inversion symmetry in the bulk space group (centrosymmetric versus non-centrosymmetric, respectively) from the presence or absence of such inversion symmetry in the atomic site point group. The latter is the subgroup formed by the subset of all symmetry operations of the crystal space group that leave that atomic site invariant[12]. The net spin polarization of a bulk crystal is the sum over all atomic sites of the local spin polarizations. One can then classify all crystal systems into three general spin polarization cases by considering different combinations of bulk space group and site point group. This is explained in the cases shown in Fig. 1a–c.

The three classes of spin polarization in nonmagnetic bulks

Absence of spin polarization (Fig. 1a). When all the site point groups contain inversion symmetry (point groups C_i, C_{2h}, D_{2h}, C_{4h}, D_{4h}, S_6, D_{3d}, C_{6h}, D_{6h}, T_h and O_h), there is no SOC-induced local spin polarization and thus the bulk spin polarization vanishes too (Fig. 1a and Table 1f). This is the case in crystal structures such as NaCl-type ($Fm\bar{3}m$), CsCl-type ($Pm\bar{3}m$), $CaTiO_3$-type perovskite ($Pm\bar{3}m$) and Mg-type hexagonal close packed ($P6_3/mmc$) structures. For example, the β-phase (NaCl-type) of SnTe—a topological crystalline insulator[13] with topologically protected states on surfaces—is found here to have vanishing spin polarization in the bulk (Table 1f). However, we will show below that such bulk spin polarization can be controlled by tuning the atomic arrangement (and, thus, the symmetry), for example changing the β-phase having no spin polarization to an α-phase having strong R-1 polarization (Table 1c).

Net bulk spin polarization: R-1 and D-1 effects (Fig. 1b). In these cases, the energy bands have non-zero net spin polarization. We next identify the pertinent combinations of bulk inversion asymmetry and site point groups leading to these macroscopic spin polarization effects (Table 1).

The D-1 effect (Table 1a,b) is associated with a non-centrosymmetric space group (bulk inversion asymmetry). In this case either all sites have non-polar point group symmetry (D_2, D_3, D_4, D_6, S_4, D_{2d}, C_{3h}, D_{3h}, T, T_d and O), or some sites have polar point group symmetry (C_1, C_2, C_3, C_4, C_6, C_{1v}, C_{2v}, C_{3v}, C_{4v} and C_{6v}) and all the site dipoles add up to zero. The simplest example (Table 1a) is the zinc-blende structure, where the bulk space group is $F\bar{4}3m$ and the site point group is T_d for both atom species, such as InAs, GaSb and GaAs (ref. 3). A similar example is the half-Heusler materials, also having bulk space group $F\bar{4}3m$ and site point group

Table 1 | Classification of spin polarization in nonmagnetic bulk materials on the basis of bulk space group and site point group.

Site point group / Bulk space group	Non-centrosymmetric (at least one site)			Centrosymmetric (all sites)
	Non-polar (all sites) (D_2, D_3, D_4, D_6, S_4, D_{2d}, C_{3h}, D_{3h}, T, T_d, O)	Polar (at least one site) (C_1, C_2, C_3, C_4, C_6, C_{1V}, C_{2V}, C_{3V}, C_{4V}, C_{6V})		(C_i, C_{2h}, D_{2h}, C_{4h}, D_{4h}, S_6, D_{3d}, C_{6h}, D_{6h}, T_h, O_h)
		Dipoles add up to zero	Dipoles add up to non-zero	
Non-centrosymmetric (for example, $F\bar{4}3m$)	**a** D-1 Example: GaAs, ZrCoBi	**b** D-1 Example: γ-$LiAlO_2$	**c** R-1 & D-1 Example: BiTeI, α-SnTe	*Not possible* (*Site point group* cannot be centrosymmetric *if space group is non*-centrosymmetric)
Centrosymmetric (for example, $R\bar{3}m$)	**d** D-2 Example: Si, NaCaBi	**e** R-2 & D-2 Example: MoS_2, Bi_2Se_3, $LaOBiS_2$		**f** Absence of spin polarization Example: β-SnTe

The point groups are given in Schoenflies notation. Site point group refers to the subset of symmetry operations of the bulk space group which transform the atomic site into itself[12]. Polar point groups are the point groups containing a unique anisotropic axis—this causes a net dipole field[9]. (In γ-$LiAlO_2$, there are dipole field induced local spin polarizations that are 'compensated' by each other, whereas the D-1 effect induces net spin polarization, that is the total spin polarization is not compensated. Thus, we do not claim compensated spin polarization in this material). When the space group is non-centrosymmetric (CS), at least one site has a non-CS point group, thus there is a Dresselhaus (D-1) spin polarization. If some of the site point groups are polar and the induced dipole fields add up to a finite amount, there is a Rashba (R-1) spin polarization. When the space group is CS, the site point groups can be all CS, in which case the spin polarization is absent, or all non-polar but some non-CS, in which case there is a D-2 compensated spin polarization, or containing polar point groups, in which case there are R-2 accompanied by D-2 compensated spin polarizations.

T_d, which have raised much interest for topological insulators[14], such as LaPdBi, LaPtBi, and ZrCoBi. The D-1 effect in these solids leads to spin splitting and, as a consequence, establishes net bulk spin polarization. As a basis for our comparison below with the new case of D-2, the D-1 behaviour is illustrated for ZrCoBi by means of DFT calculations of the band structure and spin texture in Supplementary Section A.

The R-1 effect (Table 1c) is always accompanied in bulk crystals by the D-1 effect. They originate from the combination of a non-centrosymmetric space group (bulk inversion asymmetry) with the site dipole field. Specifically, at least one site must have a polar site point group ($C_1, C_2, C_3, C_4, C_6, C_{1v}, C_{2v}, C_{3v}, C_{4v}$ and C_{6v}) and the individual dipoles add up to a non-zero value (Table 1c). Because a polar point group contains simultaneously a site dipole field and site inversion asymmetry (Table 1c), the R-1 effect in bulk crystals is always accompanied by the D-1 effect with a system-dependent relative magnitude (see below). The R-1 (accompanied by D-1) effect can occur in the following bulk structure-types: ZnS-type wurtzite ($P6_3mc$), GeTe-type ($R3m$), LiGaGe-type ($P6_3mc$), and BiTeI-type ($P3m1$). Figure 2 illustrates the R-1 and D-1 effects at both the conduction bands (CB1, CB2) and valence bands (VB1, VB2) of α-SnTe (ref. 15). Figure 2a shows the crystal structure of α-SnTe (space group $R3m$), having polar point groups C_{3v} for both the Sn and Te sites. Thus, this phase belongs to the R-1 and D-1 class in Table 1c. The calculated band structure shown in Fig. 2b reveals that R-1 and D-1 effects lift the spin degeneracy between CB1 and CB2 and between VB1 and VB2, creating a significant (∼300 meV) spin splitting. The corresponding spin textures obtained from all atoms in the unit cell are shown in Fig. 2c,d and exhibit strong spin polarization. Figure 2e,f shows more specifically a 2D view of the spin textures of CB1 and VB1 bands, illustrating the helical in-plane pattern, reflecting the dominance of R-1 over D-1 in this material. The sensitive dependence of spin-polarization classes on details of the symmetry is clearly demonstrated in the SnTe system: whereas α-SnTe in the rhombohedral $R3m$ bulk symmetry is predicted here to show a clear R-1 spin signature (Table 1c and Fig. 2), when its rhombohedral distortion (which induces polar point groups on the atomic sites) is removed by deforming the lattice to the centrosymmetric β-phase (the total energy rises by ∼0.01 eV/atom), the spin polarization disappears, as it now belongs to the unpolarized class, as illustrated in Table 1f.

Compensated (hidden) spin polarization: R-2 and D-2 effects (Fig. 1c). These can arise in crystal structures where inversion symmetry is present in the bulk space group, but not in the site point groups (Fig. 1c). This is the case when the individual sites carry either a local dipole field (for R-2) or a site inversion asymmetric crystal field (for D-2). A combination of a bulk centrosymmetric space group with a site dipole field leads to the bulk R-2 effect, whereas a combination of a global centrosymmetric space group with site inversion asymmetry results in the bulk D-2 effect (Fig. 1c). We next explain the R-2 and D-2 effects in greater detail.

The D-2 effect (Table 1d) originates from the combination of a centrosymmetric global space group with site inversion asymmetry. Specifically, all atoms have non-polar site point groups and at least one site must have an inversion asymmetric site point group ($D_2, D_3, D_4, D_6, S_4, D_{2d}, C_{3h}, D_{3h}, T, T_d$ and O). Such site inversion-asymmetry induced compensated spin polarization (D-2) can occur in a number of structure types: for example, BN-type ($P6_3/mmc$), ZrBeSi-type ($P6_3/mmc$), and diamond ($Fd\bar{3}m$) structures. Figure 3 illustrates the D-2 effect in NaCaBi, having the ZrBeSi-type structure with space group $P6_3/mmc$ and the non-centrosymmetric site point group D_{3h} for both Ca and Bi atoms, as well as the centrosymmetric site point group D_{3d} for Na atoms (Fig. 3a). The two CaBi layers connected by inversion symmetry are indicated in Fig. 3a as the α-sector and β-sector. The calculated band structure as shown in Fig. 3b clearly illustrates the large band splitting (∼400 meV) in the vicinity of the L point in the Brillouin zone between CB1 and CB2 and between VB1 and VB2. The corresponding spin texture, projected onto the real-space sectors α and β, forming the inversion partners, are shown as brown and green arrows, respectively, in Fig. 3c,d. Even though all the bands are energetically doubly degenerate as a result of bulk

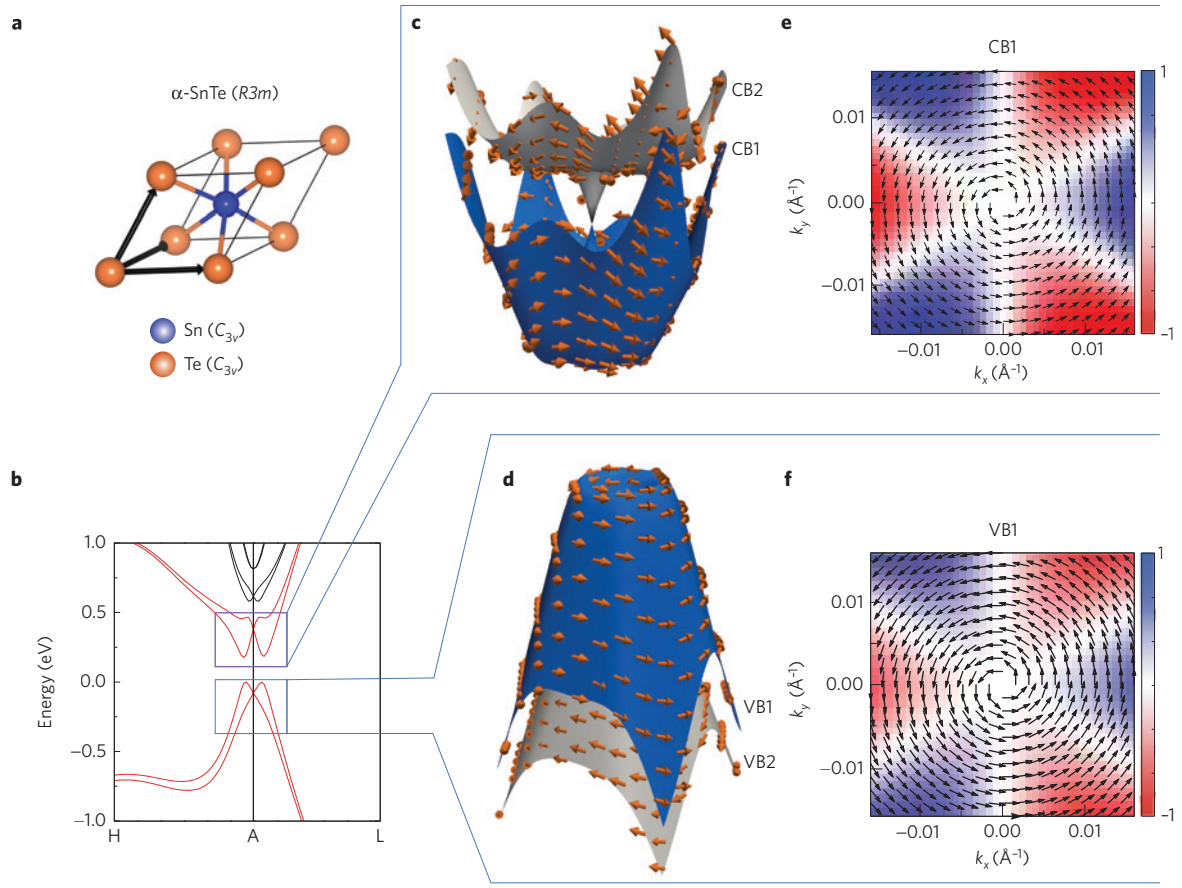

Figure 2 | Rhombohedral α-SnTe (*R3m*) with R-1 (dominant over D-1) spin textures. a, Crystal structure and site point groups of each atomic site. **b**, Band structure around the A point along the A–H and A–L directions in the Brillouin zone. The two lowest conduction bands (CB1 and CB2) and two highest valence bands (VB1 and VB2) are shown in red. **c**,**d**, Spin polarization (contributed by the entire unit cell) is represented by brown arrows for the states of spin-split CB1 + CB2 and VB1 + VB2 bands in the **k**-plane containing the A–H and A–L directions near the A point indicated by solid boxes in **b**, respectively. **e**,**f**, Corresponding 2D diagram of the spin polarizations of CB1 and VB1, respectively. The arrows indicate the in-plane spin direction and the colour scheme indicates the out-of-plane spin component. The magnitude of each spin vector is renormalized to unity for simplicity unless otherwise noted. Note that the magnitude of spin vectors varies with the **k**-points and bands depending on the strength of spin–orbit coupling and the magnitude of spin splitting.

inversion symmetry, we see that each of the branches of the two-fold degenerate band has opposite spin polarizations in real space. This real-space separation originates from the separate local site Dresselhaus SOC, as indicated by the brown branch projected on the α-sector $(CaBi)_\alpha$ layer and the green branch projected on the β-sector $(CaBi)_\beta$ layer.

Centrosymmetric bulk silicon was always assumed to be a spin polarization-free material (so it is assumed not to disturb an externally injected spin polarization[16]). It is an ideal material for long spin lifetime because the D-1 effect is absent and the effect of the nuclear spin of Si vanishes[17]. However, we illustrate in Supplementary Section B that bulk diamond-like silicon has compensated D-2 spin polarization (the class shown in Table 1d) because the site point group of Si atoms is non-centrosymmetric T_d, which leads to a local atomic Dresselhaus spin polarization.

The R-2 effect (Table 1e) is accompanied in bulk crystals by the D-2 effect. They originate from the combination of a centrosymmetric bulk space group with the 'site dipole field'. Specifically, at least one site must have a polar site point group (C_1, C_2, C_3, C_4, C_6, C_{1v}, C_{2v}, C_{3v}, C_{4v} and C_{6v}, see Table 1e). The R-2 (accompanied by D-2) spin polarization can occur in structure types such as MoS_2-type ($P6_3/mmc$), Bi_2Te_3-type ($R\bar{3}m$), and $LaOBiS_2$-type ($P4/nmm$) structures. Figure 4 illustrates the R-2 and D-2 effects at CB1, CB2, VB1 and VB2 in $LaOBiS_2$, which was recently discovered to have similar properties to cuprate- and iron-based superconductors[18]. Figure 4a shows the crystal structure of $LaOBiS_2$, having a centrosymmetric bulk space group and non-centrosymmetric polar site point group C_{4v} for Bi, S and La atoms, as well as a non-centrosymmetric non-polar site point group S_4 for O atoms. The unit cell of $LaOBiS_2$ can be divided into three sectors: two inversion-partner BiS_2 layers, termed the α-sector and β-sector in Fig. 4a, and the central La_2O_2 layer, which does not affect the low-energy (near band gap) spectrum. The calculated band structure as shown in Fig. 4b clearly illustrates large band splitting (∼120 meV) in the vicinity of the X point in the Brillouin zone between CB1 and CB2 and between VB1 and VB2. These are induced mainly by the large site dipole field as well as by the site inversion asymmetry in the BiS_2 layers. The corresponding spin textures projected on sectors α and β are shown in Fig. 4c,d. They manifest two branches of spin polarization (indicated in Fig. 4c,d by green and brown arrows) corresponding to the two BiS_2 real-space sectors shown in Fig. 4a. We see in Fig. 4c,d that the spin polarizations from the two inversion-symmetric BiS_2 layers have opposite directions and compensate each other. The 2D spin textures of CB1 and VB1 are shown in Fig. 4e,f. We see both helical (mainly in Fig. 4f) and non-helical (mainly in Fig. 4e) spin textures, suggesting that the R-2 effect is accompanied by the D-2 effect. The distribution of R-2 and D-2 effects on each band depends on the specific band character.

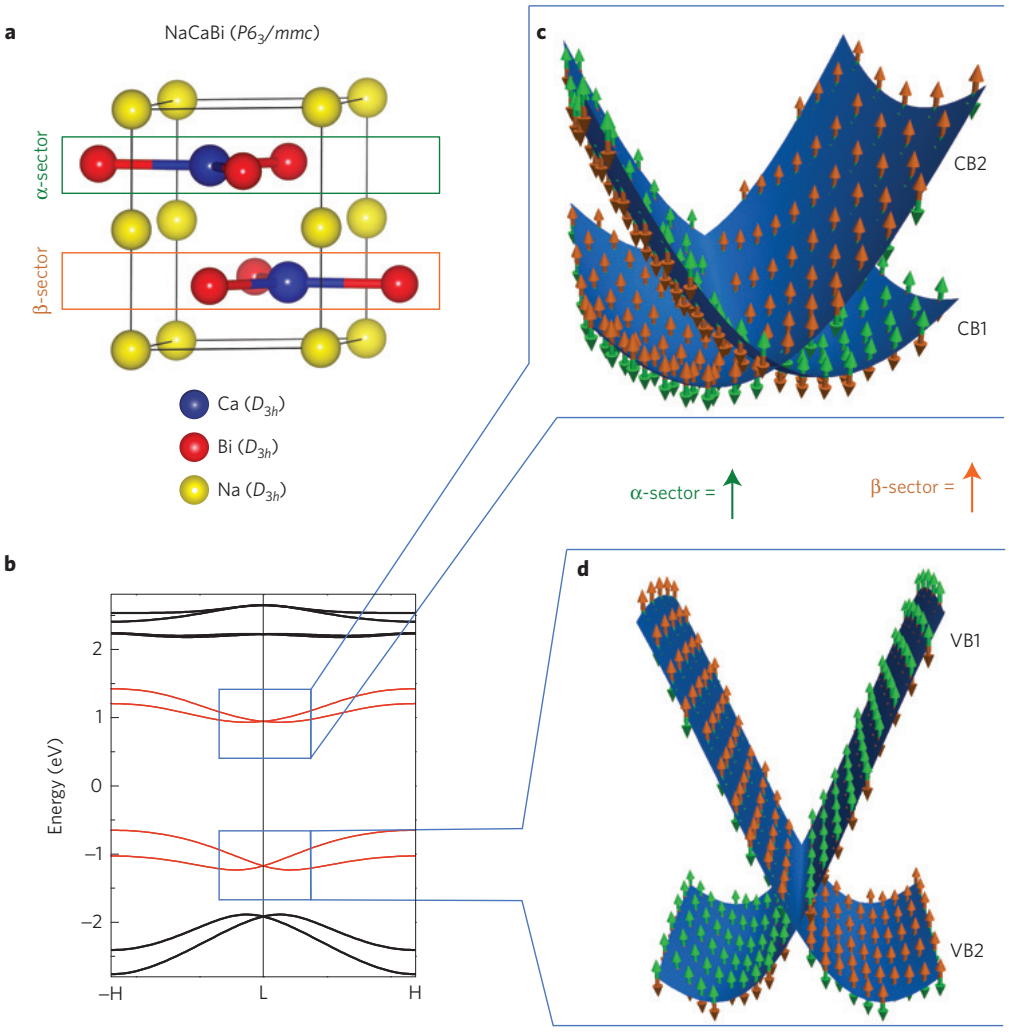

Figure 3 | NaCaBi ($P6_3/mmc$) with D-2 effect. a, Crystal structure and site point group of each atomic site. The two boxed real-space sectors (CaBi layers) forming the inversion partners used for spin projection are labelled α-sector and β-sector. **b**, Band structure near the L point along the L–(−H) and L–H directions in the Brillouin zone. The CB1+CB2 and VB1+VB2 band pairs are shown in red. **c, d**, Projected local spin polarization is represented by green (on the α-sector) and brown (on the β-sector) arrows for CB1+CB2 and VB1+VB2 bands in the **k**-plane containing the L–H and L–A directions near the L point indicated by solid boxes in **b**, respectively. The band crossing at the L point is due to both time-reversal symmetry and fractional translation operations (namely, a screw axis 6_3 and a glide plane *c* along the [0001] direction). We illustrate the compensated spin polarization near the band-crossing L point for simplicity. Note that band crossing is not necessary for compensated spin polarization.

Discussion

Physical generality of the observation. The concept that opposing local effects can mutually compensate in an extended crystal is common to the present discussion on spin polarization and a much earlier work on pyroelectricity[19] which discussed classic electro-elasticity and compensation by molecular units ('sectors'). In the present study we point out that the polar/nonpolar point group symmetry of sites carries the essential information. The connection to point group symmetry allows us to accomplish two new results. First, to identify other properties previously thought to exist only in non-centrosymmetric crystals (for example, spin polarization, piezoelectricity, and second-harmonic generation) as belonging to this general class of hidden effects in centrosymmetric crystal structures. This is demonstrated in Table 1 and Supplementary Section C, which show how these three types of observables emerge in specific combinations of site point groups and space groups. Second, the focus on site symmetries further allows us to systematically predict actual materials that would show such hidden compensation effects; for example, NaCaBi shows the D-2 effect whereas $LaOBiS_2$ shows the R-2 effect, as described in what follows.

How can one find actual materials with the R-2 or D-2 effect? Our objective is to transform the understanding of the symmetry underpinning the R-1, D-1, R-2 and D-2 effects to a search algorithm of actual materials that will manifest these effects, and then verify our understanding by calculating the respective spin texture for such prototypical materials. This is done by the following design principles: look for compounds (for example, in the Inorganic Crystal Structure Database[20]) that have centrosymmetric space groups but with at least one of the Wyckoff positions lacking inversion symmetry and belonging to either polar (for R-2) or nonpolar (for D-2) point groups (listed in Table 1). Out of the 230 space groups, 92 are centrosymmetric; out of the 32 point groups, 21 are non-centrosymmetric[19]. To find materials that have a significant R-2 or D-2 spin polarization, look for compounds that have heavy elements located on atomic sites with a large dipole field; the latter can be readily obtained from an electronic structure calculation within first-principles DFT by computing the gradient of the self-consistent electrostatic potential at various lattice sites. For $LaOBiS_2$ we find a rather large dipole field of 1.8×10^5 kV cm^{-1} on the Bi site (see details in Supplementary Section D). We find

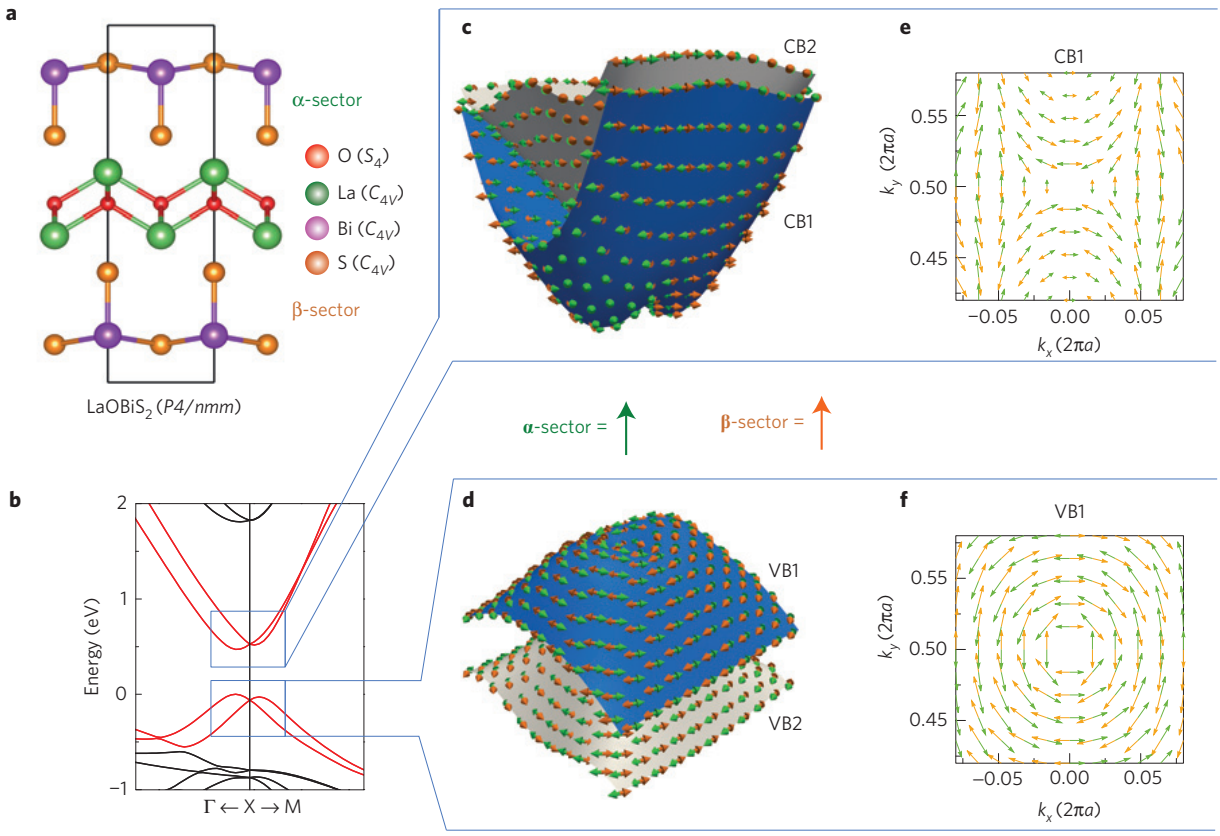

Figure 4 | LaOBiS$_2$ (*P4/nmm*) with R-2 and D-2 effects. a, Crystal structure and site point group of each atomic site. The two boxed real-space sectors (BiS_2 layers) forming the inversion partners used for spin projection are labelled the α-sector and β-sector. **b**, Band structure around the X point along the X–Γ and X–M directions in the Brillouin zone. The CB1+CB2 and VB1+VB2 band pairs are shown in red. **c, d**, Projected local spin polarization is represented by green (on the α-sector) and brown (on the β-sector) arrows for CB1+CB2 and VB1+VB2 bands in the **k**-plane containing the X–Γ and X–M directions near the X point indicated by solid boxes in **b**. **e**,**f**, 2D diagram of the spin polarization of CB1 and VB1, respectively. The arrows indicate the in-plane spin direction and *a* is the lateral lattice constant. We do not see an out-of-plane spin component in **c**–**f** to the extent of our numerical accuracy. The band crossing at the X point is due to both time-reversal symmetry and a fractional translation operation (namely, a glide plane *n* along the [110] direction). We illustrate the compensated spin polarization near the band-crossing X point for simplicity. Note that band crossing is not necessary for compensated spin polarization.

(Supplementary Section E) that layered materials having a small interaction between the layers enhance the polarization effect, as this acts to avoid the tendency for cancellation between the opposite spin polarizations from the respective layers. This is the case in $LaOBiS_2$, having a La_2O_2 barrier separating the two BiS_2 layers. As a final validation step, one can calculate the spin polarization and splitting as in Figs 3,4. The choices of the illustrative compounds in this paper—namely, $LaOBiS_2$ and NaCaBi—are inspired by these design principles, and thus their calculated spin polarizations and splittings are quite large. Therefore, our approach is not only descriptive, but also predictive.

Detectability. The real-space segregation of spin polarization in R-2 or D-2 holds the potential for detectability of such hidden spin polarization. Bulk spin polarization in such centrosymmetric layered materials could be observed when a probing beam penetrating this material along the α/β/α/β… stacking direction is attenuated with depth, so the spin polarization of layer α is not exactly compensated by the spin polarization of its inversion partner β (see a simple description in Supplementary Section E). This bulk spin effect can be distinguished from a potential surface spin effect as the former depends sensitively on the effective penetration depth of the probing beam[21] whereas the latter does not. This perspective opens the possibility of the deliberate design of imperfect compensation from different sectors to maximize the spin polarization in centrosymmetric crystals.

Potential advantages of compensated over non-compensated spin polarization. In addition to the obvious increase in the number of systems that can be amenable to spin-polarization based applications, the currently predicted spin polarization in centrosymmetric materials (the R-2 or D-2 effect) might have some advantage over the more conventional R-1 or D-1 effect in non-centrosymmetric systems. Indeed, in the former case one could sensitively manipulate the effect via the application of symmetry-breaking external perturbations such as an external electric field[22]. In contrast, the more ordinary bulk Rashba effect in non-centrosymmetric crystals (R-1) is difficult to manipulate or reverse by an external electric field because the internal field (for example, 0.4×10^5 kV cm^{-1} on the Sn site in α-SnTe, see Supplementary Section D) is usually much stronger than the external field. Thus, the hidden spin polarization may provide a new route to manipulate the electron's spin.

Methods

In this work we evaluate the band structure by density functional theory (DFT; ref. 23) using the projector-augmented wave (PAW) pseudopotentials[24] with the exchange-correlation of Perdew–Burke–Ernzerhof (PBE) form[25] as implemented in the Vienna Ab-initio Simulation Package (VASP; ref. 26). We choose the energy cutoff in the range 300–550 eV, and the reciprocal space grids of $10 \times 10 \times 10$, $18 \times 18 \times 6$, $8 \times 8 \times 6$, $12 \times 12 \times 12$ and $13 \times 13 \times 4$ for ZrCoBi, α-SnTe, NaCaBi, Si, and $LaOBiS_2$, respectively. The crystal structures are taken from refs 20,27,28 and the atomic positions are fully relaxed under a tolerance of 10^{-4} eVÅ^{-1}. Spin–orbit coupling is taken into account, although calculated by a

perturbation $\sum_{i,l,m} V_l^{SO}\mathbf{L}\cdot\mathbf{S}|l,m\rangle_{ii}\langle l,m|$ to the pseudopotential, where $|l,m\rangle_i$ is the angular momentum eigenstate of the ith atomic site[29]. The spin polarization is evaluated by projecting the calculated wavefunction $|\phi\rangle$ on the spin and orbital basis of each atomic site $C_{i,l,m,\eta}=\langle\phi|(s_\eta\otimes|l,m\rangle_{ii}\langle l,m|)|\phi\rangle$ and then summing $C_{i,l,m,\eta}$ for a given spin direction and sector that contains a number of atomic sites in the unit cell. The Wigner–Seitz radii for constructing $|l,m\rangle_i$ used in this study are listed in the pseudopotentials of the VASP simulation package[26]. In the future, we will use advanced numerical methods to project the wavefunction onto any shape of volume of the sector.

Received 6 September 2013; accepted 26 February 2014; published online 13 April 2014

References

1. Wolf, S. A. *et al.* Spintronics: A spin-based electronics vision for the future. *Science* **294,** 1488–1495 (2001).
2. Žutić, I., Fabian, J. & Das Sarma, S. Spintronics: Fundamentals and applications. *Rev. Mod. Phys.* **76,** 323–410 (2004).
3. Luo, J.-W., Bester, G. & Zunger, A. Full-zone spin splitting for electrons and holes in bulk GaAs and GaSb. *Phys. Rev. Lett.* **102,** 056405 (2009).
4. Dresselhaus, G. Spin-orbit coupling effects in zinc blende structures. *Phys. Rev.* **100,** 580–586 (1955).
5. Rashba, E. I. Properties of semiconductors with an extremum loop 1 cyclotron and combinational resonance in a magnetic field perpendicular to the plane of the loop. *Sov. Phys.-Solid State* **2,** 1109–1122 (1960).
6. Ishizaka, K. *et al.* Giant Rashba-type spin splitting in bulk BiTeI. *Nature Mater.* **10,** 521–526 (2011).
7. Di Sante, D., Barone, P., Bertacco, R. & Picozzi, S. Electric control of the Giant Rashba Effect in bulk GeTe. *Adv. Mater.* **25,** 509–513 (2013).
8. Herman, F., Kuglin, C. D., Cuff, K. F. & Kortum, R. L. Relativistic corrections to the band structure of tetrahedrally bonded semiconductors. *Phys. Rev. Lett.* **11,** 541–545 (1963).
9. Tilley, R. *Crystals and Crystal Structures* 67–79 (Wiley, 2006).
10. Winkler, R. Spin orientation and spin precession in inversion-asymmetric quasi-two-dimensional electron systems. *Phys. Rev. B* **69,** 045317 (2004).
11. Winkler, R. *Spin-Orbit Coupling Effects in Two-Dimensional Electron and Hole Systems* (Springer, 2003).
12. Flurry, R. L. Site symmetry in molecular point groups. *Int. J Quant. Chem.* **6,** 455–458 (1972).
13. Hsieh, T. H. *et al.* Topological crystalline insulators in the SnTe material class. *Nature Commun.* **3,** 982 (2012).
14. Chadov, S. *et al.* Tunable multifunctional topological insulators in ternary Heusler compounds. *Nature Mater.* **9,** 541–545 (2010).
15. Littlewood, P. B. Phase transitions and optical properties of IV-VI compounds. *Lect. Notes Phys.* **152,** 238–246 (1982).
16. Dash, S. P., Sharma, S., Patel, R. S., de Jong, M. P. & Jansen, R. Electrical creation of spin polarization in silicon at room temperature. *Nature* **462,** 491–494 (2009).
17. Zhang, L., Luo, J-W., Saraiva, A., Koiller, B. & Zunger, A. Genetic design of enhanced valley splitting towards a spin qubit in silicon. *Nature Commun.* **4,** 2396 (2013).
18. Mizuguchi, Y. *et al.* Superconductivity in novel BiS2-based layered superconductor LaO1-xF$_x$BiS2. *J. Phys. Soc. Jpn.* **81,** 114725 (2012).
19. Vaida, M. *et al.* The structure and symmetry of crystalline solid solutions: a general revision. *Science* **241,** 1475–1479 (1988).
20. ICSD. *Inorganic Crystal Structure Database* (Fachinformationszentrum Karlsruhe, Germany, 2006).
21. Cao, Y. *et al.* Mapping the orbital wavefunction of the surface states in three-dimensional topological insulators. *Nature Phys.* **9,** 499–504 (2013).
22. Liu, Q., Guo, Y. & Freeman, A. J. Tunable Rashba effect in two-dimensional LaOBiS2 films: Ultrathin candidates for spin field effect transistors. *Nano Lett.* **13,** 5264–5270 (2013).
23. Kohn, W. & Sham, L. J. Self-consistent equations including exchange and correlation effects. *Phys. Rev.* **140,** A1133–A1138 (1965).
24. Kresse, G. & Joubert, D. From ultrasoft pseudopotentials to the projector augmented-wave method. *Phys. Rev. B* **59,** 1758–1775 (1999).
25. Perdew, J. P., Burke, K. & Ernzerhof, M. Generalized gradient approximation made simple. *Phys. Rev. Lett.* **77,** 3865–3868 (1996).
26. Kresse, G. & Furthmüller, J. Efficiency of ab-initio total energy calculations for metals and semiconductors using a plane-wave basis set. *Comp. Mater. Sci.* **6,** 15–50 (1996).
27. Zhang, X., Yu, L., Zakutayev, A. & Zunger, A. Sorting stable versus unstable hypothetical compounds: the case of multi-functional abx half-Heusler filled tetrahedral structures. *Adv. Func. Mater.* **22,** 1425–1435 (2012).
28. Tanryverdiev, V. S., Aliev, O. M. & Aliev, I. I. Synthesis and physicochemical properties of LnBiOS$_2$. *Inorg. Mater.* **31,** 1361–1363 (1995).
29. Błoński, P. & Hafner, J. Magnetic anisotropy of transition-metal dimers: Density functional calculations. *Phys. Rev. B* **79,** 224418 (2009).

Acknowledgements

A.Z. is grateful to E. Rashba for important discussions on the manuscript and to M. Lahav for discussing the analogy to anti-pyroelectricity (ref. 19). This work was supported by NSF Grant No. DMREF-13-34170. X.Z. also acknowledges the administrative support of REMRSEC at the Colorado School of Mines. J.-W.L. was supported by the Center for Inverse Design, an Energy Frontier Research Center funded by the US Department of Energy, Office of Science, Office of Basic Energy Sciences, under award number DEAC 36-08GO28308.

Author contributions

X.Z. and Q.L. carried out the electronic structure calculations. A.Z. led the analysis and writing of the paper. J.-W.L. contributed equally with Q.L. and X.Z. to the preparation of the figures and writing of the paper. A.J.F. and A.Z. supervised the study.

Additional information

Supplementary information is available in the online version of the paper. Reprints and permissions information is available online at www.nature.com/reprints. Correspondence and requests for materials should be addressed to J.-W.L. or A.Z.

Competing financial interests

The authors declare no competing financial interests.